# Metrology of etched quartz and chrome embedded phase shift gratings using scatterometry

Susan M. Gaspar Wilson, S. Sohail H. Naqvi, John R. McNeil

Center for High Technology Materials
The University of New Mexico
Albuquerque, New Mexico 87131

Herschel M. Marchman

AT&T Bell Labs
Murray Hills, New Jersey 07974

Blaine Johs

J.A. Woollam Co., Inc.
650 J. Street, Suite 39
Lincoln, Nebraska 68508

Roger H. French

DuPont Central Science and Engineering
Wilmington, Delaware 19880

Franklin D. Kalk

DuPont Photomasks, Inc.
100 Texas Avenue
Round Rock, Texas 78664

**Keywords: diffraction grating, phase shift mask, scatterometry, metrology, diffraction.**

## ABSTRACT

Scatterometry is presented as an optical metrology technique potentially capable of determining the critical parameters of phase shifting diffraction grating test structures (sidewall profile, linewidth, and etch depth where appropriate). The technique is noncontact, rapid and nondestructive. The test grating structure is illuminated by a laser beam and the intensities in the different diffracted orders are measured as the angle of incidence of the laser beam is varied over a certain range.

Two different phase shifting photomasks were measured. The first mask consists of an array of chrome and chromeless phase etched gratings, fabricated at AT&T Bell Labs using e-beam techniques. The grating linewidths on this mask varied from nominal 0.5 $\mu m$ to 5.0 $\mu m$, while the etch depths varied from a nominal 190 nm to 400 nm depths. Both the chrome and the quartz gratings were measured. Linewidth and etch depth data obtained using scatterometry for the quartz gratings is presented and compared with AFM measurements of the same gratings. Each grating was measured using a Digital Instruments AFM located at AT&T. The absolute difference between the scatterometer and AFM measurements are calculated.

The second photomask is an attenuating phase shift mask fabricated by DuPont Photomasks, which utilizes an attenuating chrome film stack to produce the desired phase shift. Therefore, this photomask is not phase etched; rather the phase shift is obtained through the chrome based absorber layer. Light transmitted through the chrome lines undergoes a 180° phase shift at the exposure wavelength, relative to the light transmitted through the adjacent quartz spaces. The linewidth and line profile of the chrome grating was determined using scatterometry.

The measurements of the diffracted orders were made using the $2\theta$ scatterometer located at the University of New Mexico. The shape of the diffraction curves obtained in this manner has been shown to be sensitive to the grating structure parameters (sidewall profile, etch depth, linewidth, etc.).[1,2,3] An estimate of the quartz phase etched structure parameters and the attenuating

chrome grating parameters was obtained through a combination of rigorous coupled wave theory (RCWT) and minimum mean square error (MMSE) analysis. Finally, the long term and short term repeatabilities of the scatterometer measurements are shown to be excellent.

## 2.0 BACKGROUND

The lithographic process is the technical driver of the semiconductor industry. In a presentation given by K. Brown of SEMATECH at the 1994 BACUS conference, she comments that "Mask technology will continue to be a *key enabler* of the total lithographic system... independent of other technology alternatives". With so much emphasis being placed on mask technology, there is also additional emphasis being placed on the development of inspection tools for the photomask industry. One active area of research is in the development of inspection tools for characterizing photomasks.

The theory of PSMs has been covered widely in the literature.[6] Basically, phase shifting photomasks utilize interference of adjacent diffracted fields from closely spaced apertures which are optically 180° out of phase. The phase shift of 180° can be obtained by either depositing onto one aperture a transmissive layer of thickness d, given by,

$$d = \frac{\lambda}{2(n-1)}, \qquad 1$$

or etching one of the apertures to a depth, d. The wavelength, $\lambda$, is that used during wafer exposure and $n$ is the index of the transmissive shifter material. The performance of the phase shifted area depends upon the actual etch depth (or thickness), the linewidth, the sidewall angles, the line profile, and the alignment of the shifter to the apertures (in the case of a deposited layer). Photomask metrology tools must therefore address the measurement of these critical parameters.

## 3.0 SAMPLE DESCRIPTION

### 3.1 AT&T Photomask

The first phase shifting photomask used in this work was fabricated by AT&T Bell Labs. The photomask is a standard Hoya five-inch square, 90 mils thick photomask with a chrome oxide on chrome film stack deposited on a quartz substrate. The photomask layout consists of a matrix of 48 e-beam written gratings. Figure 1 is a schematic of the mask layout as described below. There are four columns of different linewidths, with nominal 50/50 line to space ratios, which are repeated yielding eight columns in total. The smallest nominal linewidth was 0.5 $\mu m$, followed by a 1.0 $\mu m$ linewidth, a 2.0 $\mu m$ linewidth, and finally a 5.0 $\mu m$ linewidth. The six rows represent different levels of etch depth from a nominal 190 nm etch to a nominal 400 nm etch. At each row and column position, there are four 5mm by 5mm size gratings, two of which are etched chrome on etched quartz and two are simply etched quartz. Reactive ion etch (RIE) processing of the photomask helped to ensure vertical sidewall structure. Further, at each location one pair of quartz and chrome gratings were written with vertical lines while the other pair of gratings have horizontally written lines. The data and results presented in this paper are for the gratings with vertical lines exclusively.

### 3.2 DUPONT EMBEDDED PHASE SHIFT PHOTOMASK

The second photomask is a chrome embedded phase shift photomask produced by DuPont Photomasks. The structure of interest on the photomask is a large area (2 cm by 2 cm) composed of a series of diffraction gratings (78 in total) each of which is 2 cm wide by 150 $\mu m$ high. The grating lines are 150 $\mu m$ long. The specific grating structure and material parameters are discussed fully in later sections.

## 4.0 THEORETICAL MODEL FOR SCATTEROMETRY

The scatterometry technique for measuring grating parameters is a two fold process: first, measuring the scatter from the grating, and second, finding a grating model which fits the experimental data. The solution to the second part, finding the appropriate grating model, requires one to be able to compute the scatter from a hypothetical structure. The accuracy in modeling the physical structure with a hypothetical structure is contingent upon how well the grating material parameters are known at the probe wavelength of the scatterometer. In the case of a chrome grating, knowledge of the real and imaginary parts of the index of refraction and the thickness of the chrome oxide and chrome layers are essential for an accurate model. Details of how the material parameters for the chrome gratings are determined is addressed in a separate section. For the simpler case of an etched quartz (fused silica) grating, only the complex index of refraction of the quartz material is necessary and is easily obtained. In both cases, the scatter from the hypothetical structure is computed using rigorous coupled wave theory[8,11] (RCWT), which is discussed

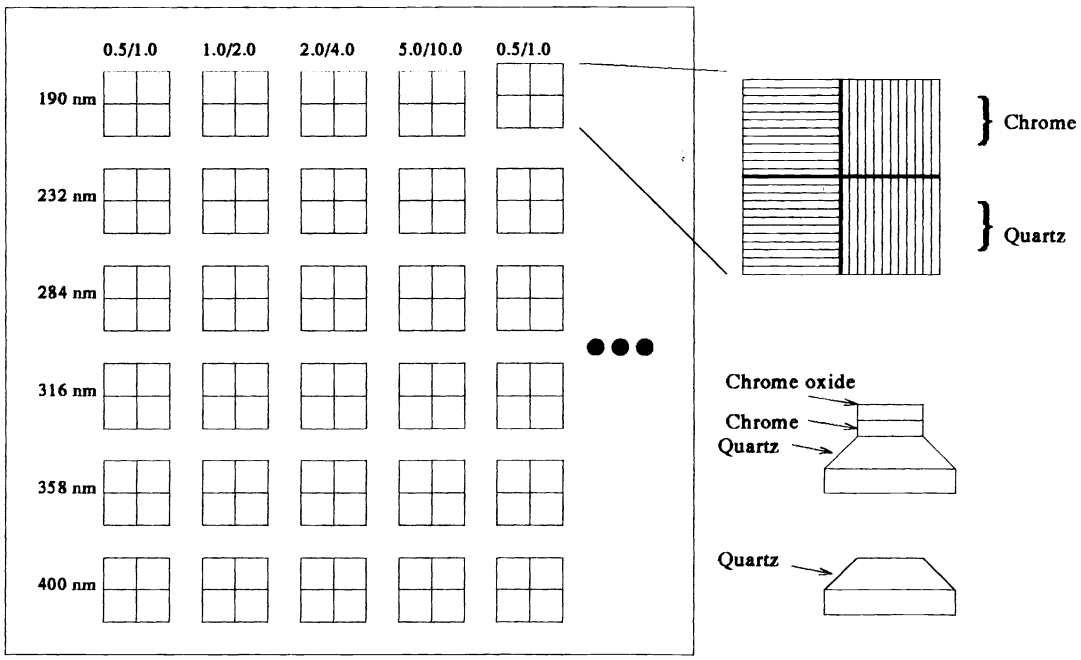


Figure 1. AT&T photomask layout.

in a later section.

The modeling of the etched quartz gratings will be discussed first; the chrome gratings which require more extensive modeling are discussed last.

## 4.1 QUARTZ GRATINGS

The first step in modeling the quartz gratings is to determine the index of refraction of the quartz material at 6328 Å, the wavelength of the scatterometer laser source. The real part of the index, n, is found to be 1.45 and the complex term, k, is small enough to be assumed equal to zero[6]. The complex portion of the index is often assumed to be zero for dielectrics, such as quartz.

The second step in modeling is to develop the approximate geometry of the quartz grating structure. Figure 2 shows the simplest grating profile, consisting of lines with 90° sidewall angles, as well as the grating parameters to be determined in the analysis. The grating structure is divided into three different regions. Region I includes the space above the grating and region III consists of the quartz substrate, which is assumed to be infinite in extent. More will be said about this assumption of an infinitely thick substrate in the experimental section. Region II, where the actual grating lies, is described in the theory by a number of grating "slices". For the simple case of perfectly straight sidewalls, the grating can be adequately described by one slice having a thickness equal to the depth of the quartz trench.

If, on the other hand, the grating line has a rounded top corner profile, as shown in Figure 3, then one can slice the structure into layers with varying thicknesses and widths to best approximate the actual profile. Clearly, the more slices that are used the better the structure is approximated, with the tradeoff being increased computational time. One must determine what level of approximation is acceptable or required.

The rounded corner profile was used to model the etched quartz gratings on the photomask. The corner was approximated as a quarter circle with a radius of 0.07 $\mu m$, as shown in Figure 3. Thirty slices were used to approximate this quarter circle profile. The remainder of the line was modeled as a single slice with 90° sidewall angles. The initial guess of the corner radius was

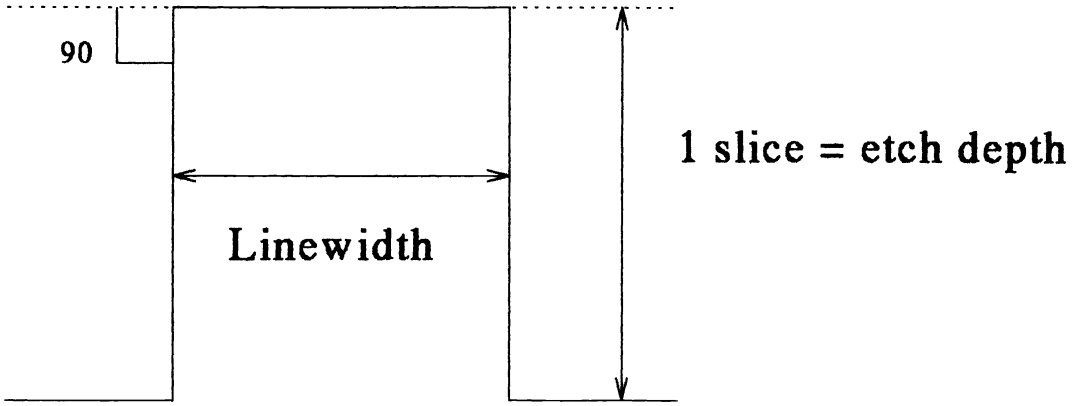


Figure 2. Quartz grating profile.

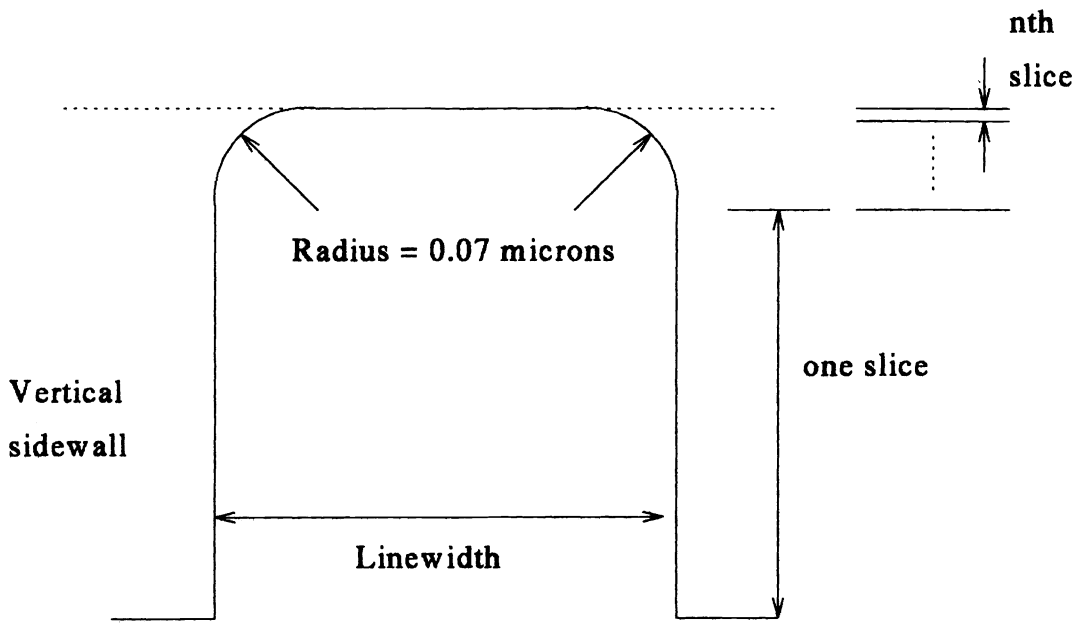


Figure 3. Quartz rounded top corner profile.

based upon measurements of the corner radii from a cross sectional SEM photograph taken on a similar photomask processed concurrently with this photomask. The rounding of the corners occurred due to the processing and appears to be of the same magnitude regardless of the linewidth. Therefore, the same radius of curvature was used to model all the quartz grating linewidths. The difference that the rounded corner profile makes compared to the squared off corner is represented in Figure 4. The plots represent the computed intensity of the reflected 0th order as a function of the angle of incidence for the square corner and the rounded corner with a radius of 0.07 $\mu m$ on a 0.68 $\mu m$ line, 1 $\mu m$ pitch grating. Also included in the plot is the experimental data for the quartz grating. The better fit which is obtained between the experimental curve and the rounded corner profile verifies the use of the profiling technique.

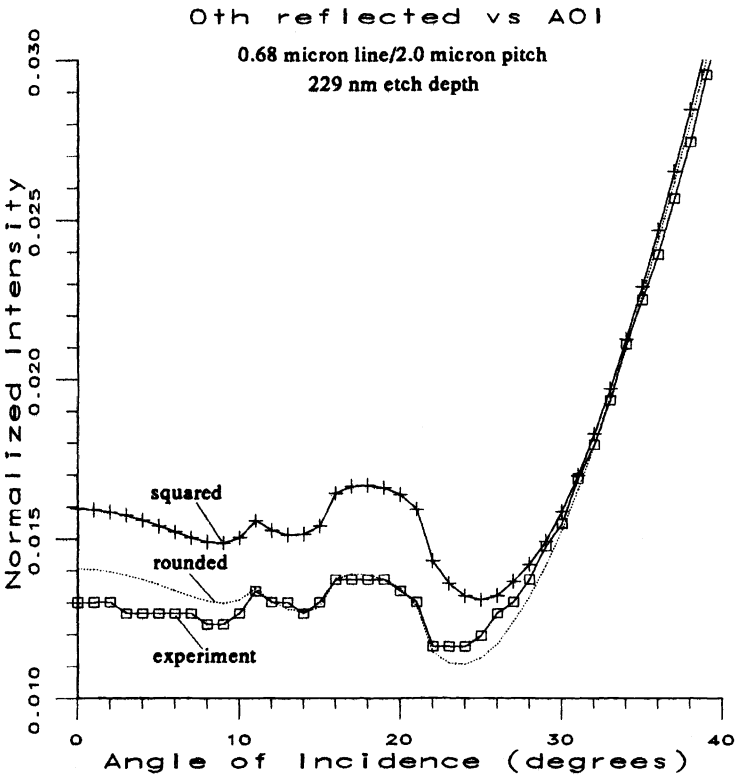


Figure 4. Effect of rounded top corner on theory.

## 4.2 CHROME GRATINGS

There are two basic types of chrome used in photomask production presently: conventional chrome and transmissive chrome. Conventional chrome photomasks have an opaque layer of chrome usually 800 to 1200 Å thick, and is used exclusively for its attenuating properties. Transmissive chrome is not opaque but transmits some of the incident radiation. One can attain phase shifts (the standard is 180° between chrome lines and adjacent quartz spaces by controlling the optical parameters (thickness, n, k, index profile) of the chrome layers. Additionally, the exposure wavelength of the stepper determines the required chrome transmission. For the mercury line at 436 nm (g-line) the chrome transmission must be adjusted to obtain a 180° phase shift with respect to the adjacent quartz space. The mercury line at 356 nm (i-line) requires different chrome transmission characteristics since the phase shift depends inversely with the exposure wavelength, as seen in Equation 1.

The analysis of the scatter from chrome diffraction gratings is more difficult than for etched quartz gratings due to the complex composition of the chrome oxide and chrome layers. In practice, chrome is used more extensively than plain quartz in designing phase shifting structures. Therefore, the analysis of attenuating chrome gratings is quite important. The determination of the thickness and the complex index of refraction of the chrome oxide and the chrome layers is an extensive research project in its own right.

The DuPont Corporation, working with the J. Woollam Company was able to successfully model attenuating chrome photomasks for use with both i-line and g-line exposure wavelengths[10]. DuPont has agreed to share their depth profiles which model the complex index of refraction of the chrome oxide and chrome films as a function of depth. A summary of their work is presented in order to give the background necessary to understand how the depth profile was obtained. The validity of the depth profile is critical in obtaining accurate results from the RCWT calculations.

## 4.3 DETERMINATION OF DUPONT CHROME AND CHROME OXIDE MATERIALS PARAMETERS

The chrome oxide and the chrome layers are graded index materials which satisfy specific requirements for the transmission characteristics at the exposure wavelength. The composition of the sputtered chrome is altered during deposition through control of the input gas mixture (oxygen, nitrogen, and carbon are used) and the cathode power. Additionally, the etch characteristics of the chrome oxide and chrome layers can be altered via the composition of the film. The graded, complex index of refraction profile is approximated by a finite number of different levels each of a constant index for a specific wavelength.

Johs, et al.[9] was able to determine the complex index of refraction of the chrome oxide and chrome films as a function of depth. The chrome oxide/chrome layer was modeled as a single, graded-index film with nominal thickness of 128.0 nm. The film, which in actuality is a complex mixture with its composition varying on an Angstrom level, can be modeled as a single film composed of metal-like and dielectric-like components which vary as a function of depth. The surface of the film can be expected to be more dielectric while near the substrate interface, the film would be more metallic. By varying the fractions of the dielectric and metallic materials, one can adjust the index of the film to match both reflected and transmitted ellipsometric and spectroscopic data. This type of approach is called an Effective Medium Approximation (EMA). Bruggeman[6] developed a model based on this form which is valid for films where one can safely assume there is uniform mixing of the constituents on a scale which is small compared to the wavelength of light used to do the index analysis.

Johs, et al. then developed a "seed" model from this preliminary data and iteratively adjusted it to match variable angle spectroscopic ellipsometry (VASE) and optical spectroscopy data. The final depth model is shown in Table 1. There are 10 levels of unequal thickness and different optical constants which describe the grating stack for an incident wavelength of 635 nm. The optical constants profile forms the basis of the grating structure which is used as input into the coupled wave theory. The geometric grating parameters are solved for while the depth profile remains a constant. The variables being sought are therefore linewidth, sidewall angle, and line profile.

## 5.0 COUPLED WAVE MODEL

After the mask structure of interest has been divided into different regions and the grating lines have been sliced appropriately, the electromagnetic (EM) field within each of the three regions is expressed as a sum of plane waves with unknown field amplitudes. In region II, where the grating is located, the EM field is expanded as a sum of inhomogeneous plane waves. Next, the periodic refractive index within region II (quartz line adjacent to an air space) is expanded in a Fourier series. State variable techniques are then implemented to solve the wave equation expansion in each grating slice. Finally, the boundary conditions on the tangential electric and tangential magnetic fields are invoked which result in coupled linear equations. These linear equations are then solved using matrix based methods, yielding the electric and magnetic field amplitudes. The reflected and transmitted diffraction order efficiencies are then obtained from the field amplitudes.

| Layer | n | k | thickness(Å) |
|---|---|---|---|
| 1 | 2.0237 | 0.00037053 | 161.8 |
| 2 | 2.2462 | 0.11189 | 161.78 |
| 3 | 2.4773 | 0.24191 | 161.8 |
| 4 | 2.7144 | 0.37855 | 161.79 |
| 5 | 2.9543 | 0.51233 | 161.79 |
| 6 | 2.9543 | 0.51233 | 94.21 |
| 7 | 2.8184 | 0.43738 | 94.21 |
| 8 | 2.6828 | 0.36051 | 94.20 |
| 9 | 2.5484 | 0.28298 | 94.21 |
| 10 | 2.4156 | 0.20648 | 94.208 |

Table 1. Stack parameters for chrome film.

The strategy employed to solve the grating parameter identification problem is an based on iterative refinement. First, the grating is assumed to be of a certain generic shape of unknown control parameters. Often one has a fairly accurate idea of what the structure should be. After one has determined a specific geometry, the associated diffraction order efficiencies are computed and compared with the measured values. The hypothetical geometry is then adjusted, the diffraction efficiencies recomputed and the process repeated until one achieves satisfactory convergence.

One approach to the parameter identification problem is to generate an extensive set of diffraction data over a likely range of perturbations for each of the parameters of interest. The experimental data for a specific grating is compared to the large data set to find the "best match". The definition of "best match" depends upon the statistical analysis technique felt to be the most robust indicator of a match between experiment and theory. In our case, we have had great success using the simple approach of minimum mean square error (MMSE) to define the "best match" of the data. One likely reason this technique has worked so well for our data is that the theoretical grating model approximates the experimental data extremely well.

## 6.0 EXPERIMENTAL PROCEDURE

The experimental apparatus which was used to make the scattered light measurements is a research grade optical scatterometer located at the University of New Mexico. The instrument arrangement is shown schematically in Figure 5. Light from a TE polarized He-Ne laser passes through a spatial filter, a chopper, and is focused by a lens before finally passing through a neutral density filter. The beam waist can be adjusted at the sample by moving the lens. For the measurements taken on the AT&T photomask, the focus was adjusted so that each diffraction order was fully contained within 70% of the detector's active area for all angles of incidence. The size of the incident beam on the grating was approximately 500 $\mu m$ measured at the $1/e^2$ distance.

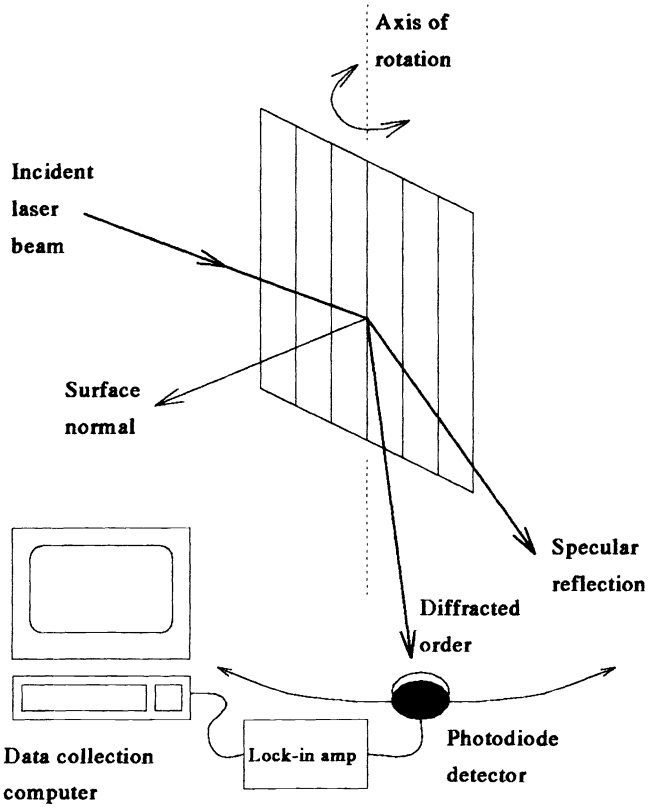


Figure 5. Research grade scatterometer.

Measurement of the attenuating chrome grating on the DuPont photomask required a beam waist of approximately 125 $\mu m$ measured at the $1/e^2$ distance. This was due to the small grating size, approximately 2 cm wide by 150 $\mu m$ high. The distance from the sample to the detector was kept constant for all measurements.

The diffracted orders from the grating are scanned with a photodiode which rotates in the plane of incidence. The signal from the photodiode is then fed thorough a transimpedance amplifier before demodulation by a lock-in amplifier. The signal intensity vs angle measurement is subsequently stored in a computer for later analysis.

The sample is located on a high resolution rotary stage which allows the angle of incidence to be varied by rotating the sample. The stage is capable of angular resolution of 0.0016° and was rotated over an angular range for which the diffracted order of interest existed. Similarly, a detector is mounted on a movable arm connected to a second high resolution rotary stage having its axis coincident with the first. Therefore, the intensity in one diffracted order may be measured as a function of the angle of incidence. This version of the scatterometer is known as the $2\theta$ scatterometer since two angles are involved in the measurement. Figure 6 shows an example of how the intensity in the 0th reflected order changes as a function of angle of incidence for a given etch depth. Each etch depth has a unique intensity profile which is then exploited by the analysis in determining the grating etch depth.

The rotating detector is a silicon photodiode with an active area of approximately 5 $mm^2$ . The detector is mounted with a declination angle of 5° to reduce reflections from the front of the detector surface back onto the sample. Additionally, a black absorbing cover was fitted to the front of the sample limiting the measurement area to the grating region of interest. An open sample mount was designed to support the mask along its perimeter which allows the transmitted diffracted orders to travel

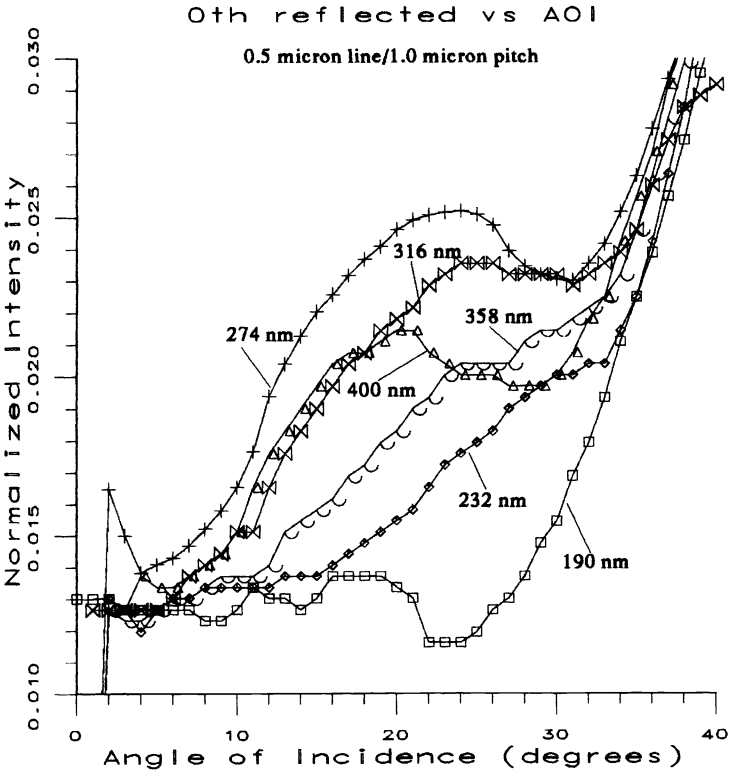


Figure 6. Experimental $0^{th}$ reflected diffracted order for different etch depths.

undeviated. Suitable precautions must be taken to reduce back reflections from the substrate during the measurement process. Elimination of the back reflections is essential if an infinite substrate model is used in the analysis.

A measurement of the total power incident on the grating is also made, which allows the fraction of total power diffracted into the different orders to be accurately determined. This normalization procedure also reduces the effect of any day-to-day power fluctuation in the laser output on the intensity measurements.

## 6.0 AT&T PHOTOMASK RESULTS

The etched quartz phase shifted gratings on the AT&T photomask were measured using the $2\theta$ scatterometer described in the experimental section. A model of the grating was developed and RCWT was used to solve for the diffracted order efficiencies as a function of the angle of incidence. Diffraction data was generated over the parameter range of interest, and the minimum mean square error (MMSE) criterion was used to determine the grating parameters. All the predictions for the AT&T grating linewidths and etch depths reported in this paper were made using the 0th reflected diffracted order exclusively.

There are four columns with gratings of different linewidths arranged on the photomask covering the range of nominal 0.5 $\mu m$, 1.0 $\mu m$, 2.0 $\mu m$ and 5.0 $\mu m$. All the gratings are nominal 50/50 line/space. The AFM measured values for the linewidths were used as an approximate guide in order to reduce the theoretical search space. The ranges for the linewidths and the etch depths over which the diffraction code was run is summarized in Table 2.

The four grating pitches take different amounts of computation time. The computation time is dependent upon the number diffracted orders which must be maintained during the calculations to achieve convergence. For the 1 $\mu m$ pitch, only three orders (propagating and evanescent modes combined) need to be retained, whereas for the 10 $\mu m$ pitch, 20 orders must be retained in the computation. The search space for the larger pitched grating (4 and 10 $\mu m$ pitches) is modified accordingly to ensure that the full range of possible etch depths is covered, but is accomplished in stages.

The overall range of etch depths covered in the first data set for all 4 pitches was from 150 nm to 500 nm, in steps of 10 nm. The linewidth ranges were based upon the AFM linewidth measurements and on average spanned a 0.1 $\mu m$ space in steps of 0.01 $\mu m$. After the first data set was completed, predictions were made on the grating linewidths and etch depths using MMSE. A second set of diffraction data was generated for the 1 and 2 $\mu m$ pitch gratings over smaller ranges, based upon the results of the first prediction. Therefore, 1 nm resolution was obtained over a 10 nm wide range centered about the first etch depth prediction.

The scatterometer measurement results for linewidth and etch depth are presented in Tables 3 and 4, respectively, with the corresponding AFM measurements. A Digital Instruments AFM was run in tapping mode at AT&T where the measurements were made. The cantilever probe was fabricated out of silicon and was pyramidal in shape. Also included in the Table is the absolute difference between the scatterometer and AFM measurements. Two grating locations were inadvertently skipped in making the AFM etch depth measurements; and one grating location was inadvertently skipped while making the scatterometry measurements.

| Nominal grating linewidth | Linewidth range (microns) 1st prediction | Linewidth range (microns) 2nd prediction | Step size for linewidth (microns) | Etch depth range (nm) 1st prediction | Step size for etch depth (nm) 1st prediction | Step size for etch depth (nm) 2nd prediction |
|---|---|---|---|---|---|---|
| 0.5 | 0.6 to 0.7 | - | 0.01 | 150 to 500 | 10 | 1 |
| 1.0 | 1.0 to 1.1 | - | 0.01 | 150 to 500 | 10 | 1 |
| 2.0 | 1.98 to 2.04 | 1.94 to 1.97 | 0.01 | 150 to 500 | 10 | 1 |
| 2.0 | 1.98 to 2.04 | 2.05 to 2.08 | 0.01 | 150 to 500 | 10 | 1 |
| 5.0 | 5.05 to 5.12 | 5.00 to 5.04 | 0.01 | 150 to 500 | 10 | 1 |
| 5.0 | 5.05 to 5.12 | 5.13 to 5.15 | 0.01 | 150 to 500 | 10 | 1 |

Table 2. Range of linewidths and etch depths for quartz search space.

| Nominal grating linewidth (nm) | Scatterometer MMSE measurement (nm) | AFM measurement (nm) | Difference (nm) |
|---|---|---|---|
| 0.5 micron line | | | |
| 190 | 0.68 | 0.62 | +0.06 |
| 232 | 0.68 | 0.66 | +0.02 |
| 274 | 0.68 | 0.66 | +0.02 |
| 316 | 0.69 | 0.66 | +0.03 |
| 358 | 0.68 | 0.66 | +0.02 |
| 400 | 0.66 | 0.66 | 0.00 |
| 1.0 micron line | | | |
| 190 | 1.02 | 1.04 | -0.02 |
| 232 | 1.09 | 1.04 | +0.05 |
| 274 | 1.07 | 1.02 | +0.05 |
| 316 | 1.10 | 1.03 | +0.07 |
| 358 | 1.10 | 1.05 | +0.05 |
| 400 | 1.10 | 1.04 | +0.06 |
| 2.0 micron line | | | |
| 190 | 2.08 | 2.00 | +0.08 |
| 232 | 1.98 | 2.01 | -0.03 |
| 274 | 1.98 | 2.00 | -0.02 |
| 316 | 1.97 | 2.01 | -0.04 |
| 358 | 1.97 | 2.02 | -0.05 |
| 400 | 1.98 | 2.01 | -0.03 |
| 5.0 micron line | | | |
| 190 | 5.13 | 5.07 | +0.06 |
| 232 | 5.04 | 5.08 | -0.05 |
| 274 | 5.15 | 5.10 | +0.05 |
| 316 | 5.02 | 5.10 | -0.08 |
| 358 | 5.04 | 5.08 | -0.04 |
| 400 | 5.15 | 5.12 | +0.03 |

Table 3. Linewidth results for quartz gratings.
Linewidth bias = 0.01 $\mu m$
$3\sigma$ = 0.15 $\mu m$

| Nominal grating etch depth (nm) | Scatterometer MMSE measurement (nm) | AFM measurement (nm) | Difference (nm) |
|---|---|---|---|
| 0.5 micron line | | | |
| 190 | 229 | 232 | -3 |
| 232 | 269 | 278 | -9 |
| 274 | 294 | 306 | -12 |
| 316 | 410 | 374 | +36 |
| 358 | 449 | 413 | +36 |
| 400 | 485 | * | - |
| 1.0 micron line | | | |
| 190 | 232 | 235 | -3 |
| 232 | 275 | 281 | -6 |
| 274 | 320 | 326 | -6 |
| 316 | 381 | 376 | +5 |
| 358 | 420 | 416 | +4 |
| 400 | 460 | * | - |
| 2.0 micron line | | | |
| 190 | 233 | 240 | -7 |
| 232 | 279 | 276 | +3 |
| 274 | 320 | 329 | -9 |
| 316 | 375 | 378 | -3 |
| 358 | 415 | 410 | +5 |
| 400 | 450 | 457 | -7 |
| 5.0 micron line | | | |
| 190 | 232 | 240 | -8 |
| 232 | 277 | 285 | -8 |
| 274 | 313 | 329 | -16 |
| 316 | 366 | 365 | +1 |
| 358 | 412 | 396 | +16 |
| 400 | 448 | 449 | -1 |
| * Missing AFM data | | | |

Table 4. Etch depth results for quartz gratings.
Etch depth bias = +0.36 nm
$3\sigma$ = 39.6 nm

The AFM linewidth measurement technique has an estimated uncertainty of ±0.05 to 0.1 $\mu m$. This is primarily due to effects of the unknown probe tip shape on the linewidth measurement. Similarly, the estimated uncertainty for the AFM etch depth measurements is ±5 to 10 nm. The average absolute difference between the scatterometer and AFM measurements of the linewidth is 0.04 $\mu m$. Therefore, the scatterometer linewidth measurements are within the uncertainty of the AFM.

The average absolute difference between the two sets of measurements of etch depth (including all depths measured) is 10 nm. The 1 $\mu m$ pitch gratings etched to nominal 316 nm and 358 nm depths were measured to be deeper by the scatterometer than the AFM. Comparison of the theoretical best fit data and the scatterometer data shows that the actual gratings may have other structural differences which are manifesting themselves in the scatter signature. Additional measurements by both the

scatterometer and the AFM should be able to resolve the measurement differences in the two etch depths.

### 6.1 REPEATABILITY

Short term and long term repeatability of the scatter measurements were investigated. To measure short term repeatability, the photomask was positioned in the sample mount and 15 consecutive measurements were made on one of the 1 $\mu m$ pitch gratings without the mask being repositioned. Linewidth and etch depth predictions were made on all of the intensity scans and were identical to within the resolution of the theory (i.e. within the step size used to generate the range of theoretical files). Additionally, the average rms difference of the 15 consecutive measurements was calculated to be $1.26X10^{-4}$. The rms difference was also calculated between measurements taken in June 1994 and August 1994, during which time the scatterometer underwent considerable structural changes. The long term repeatability as given by the rms difference between the two measurements and is calculated to be $3.56X10^{-4}$.

### 6.2 ATTENUATING PHASE SHIFT PHOTOMASK

The DuPont attenuating phase shift photomask presented different problems in the modeling phase. The grating structure of interest on the photomask was known to have nominal 2.0 $\mu m$ linewidth and 4.0 $\mu m$ pitch. Other structural information such as the sidewall profile was not known. Therefore, a few assumptions had to be made about the profile in order to reduce the search space of possible solutions.

This particular photomask was processed using wet etch techniques. One of the characteristics of a wet etched chrome line is the presence of an undercut sidewall profile. Wet etching proceeds in an isotropic manner which means that the etching process occurs at a similar rate in all directions. Therefore the structure is etched in a vertical direction as desired, but also in a lateral direction. Often, though, the undercutting of the sidewall results in improved edge definition of the transferred pattern into photoresist. The amount of undercut is therefore an important parameter to be able to detect and to measure. The ability to measure the sidewall profile would help to enable consistent processing results.

The line profile which is used to model the structure was assumed to have an undercut sidewall profile. For simplicity, the line structure is taken to be symmetric; the depth profile provided by DuPont fixes the height of the structure and its composition. There is nothing in coupled wave theory which precludes asymmetric profiles from being analyzed, but this represents a further refinement to the basic profile. Figure 7 details the line profile which was used to model the chrome lines. Note that the Figure is for illustration only, and the dimensions are not to scale. The amount of undercutting was first considered to be equal in the lateral and vertical directions. This assumption was later refined, leaving a portion of the oxide-like layer at the top not undercut. It is possible then to define a separate "chrome linewidth" which refers to the undercut layers of metallic-like material underneath the oxide layer. A coordinate system is defined at the bottom edge of the oxide overhang with the y-axis pointing down and the x-axis pointing rightward. Using this coordinate system the amount of undercut in the x direction at a specific height, y, can be expressed in the form

$$x = A(\cos(fy + b) + c)^q.$$

Any number of possible forms could be used; the choice of this functional form is somewhat arbitrary. There are certain constraints on the appropriate shape of the curve as well as the boundary conditions which help to narrow the choices. The $A$ coefficient in the equation refers to the maximum amount of undercut at $y = 0$. The frequency of the cosine, $f$, the phase term, $b$, the offset, $c$ and the power $q$, are all adjusted until a suitable representation is obtained of the sidewall profile. Clearly, this is a subjective as well as iterative technique; but for lack of further information on the line profile, there is little alternative.

The attenuating chrome line profile proved to be more complex to model than the simple etched quartz gratings on the AT&T photomask. It was necessary to match the 0, +1st, and +2nd diffracted reflected orders in attempting to fully describe the line structure. The "best fit" was chosen by graphical comparison of each order with its corresponding experimental data. Figure 8 shows the comparison of the experimental data for the 0th and +1st diffracted reflected orders and the "best fit" theoretical data. Figure 9 shows the experimental and theoretical data for the +2nd order. The line profile used to generate this theoretical data is discussed below.

The theoretical calculations for the attenuating chrome gratings take much longer than for the etched quartz gratings due to the increased complexity of the chrome film stack and the required number of diffraction modes which must be retained in the analysis in order to obtain proper convergence of the solution. Time constraints limited the number of possible theoretical structures which could be modeled, and therefore prohibited using the Minimum Mean Square Error criterion to find the "best fit". The fact that the theoretical data for three diffraction orders match the experimental

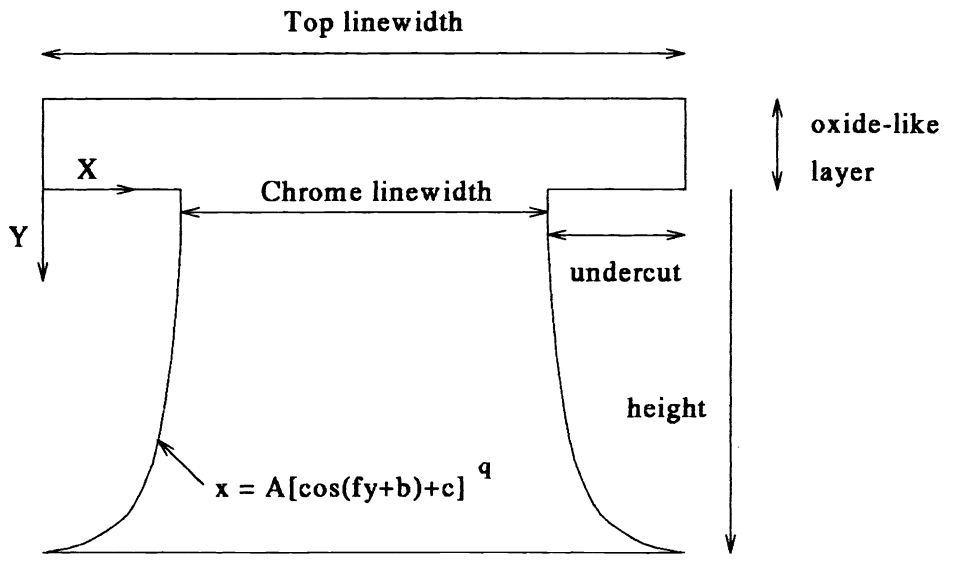


Figure 7. Line profile used to model chrome line.

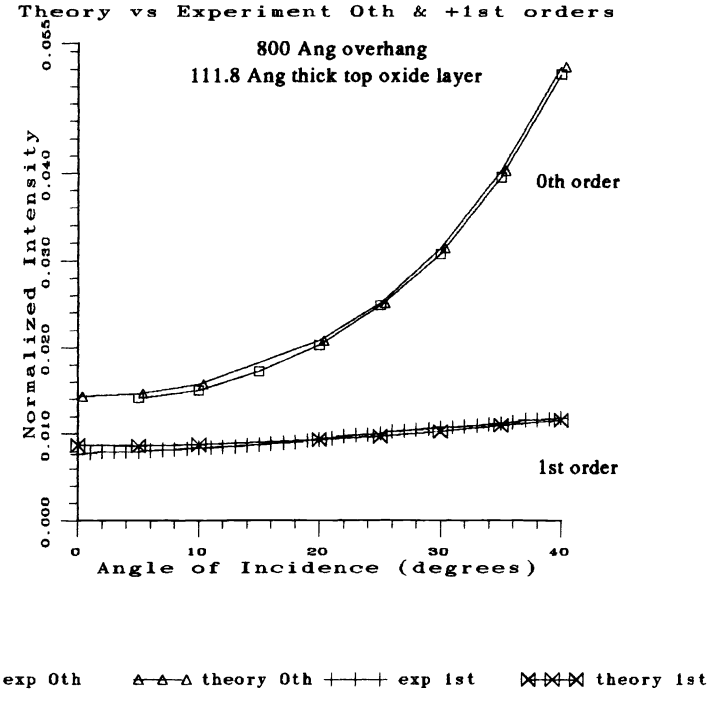


Figure 8. Experimental and theoretical data for $0^{th}$ and $1^{st}$

data so well lends quite a degree of confidence to the theoretical profile identified by the search.

After many iterations, the best fit was found for the undercut chrome profile and is shown in Figure 10. The linewidth is 2.0 $\mu m$ with the top oxide layer having a thickness of 111.8 Å. The amount of lateral undercut is 800 Å and the height of the undercut region is 956 Å. After discussions with the process engineer who fabricated this photomask, this line profile was deemed realistic. Further refinement of the line profile could be done, for example, rounding of the corners of the top oxide layer. Cross-sectional SEM photographs are planned in the future to help validate this line profile obtained non-destructively using scatterometry.

## 6.3 REPEATABILITY

Short term repeatability studies were carried out on the attenuating chrome grating measurements. Short term repeatability refers to consecutive measurements made on the same grating without repositioning the photomask. To measure short term repeatability, the photomask was positioned in the sample mount and 25 consecutive measurements were made on one of the chrome gratings without the mask being repositioned. Linewidth and etch depth predictions were made on all of the 25 intensity scans and were identical to within the resolution of the theory (i.e. within the step size used to generate the range of theoretical files). Additionally, the average rms difference of the consecutive measurements was calculated to be $9.58X10^{-5}$. Long term repeatability could not be determined due to the time constraints on this research.

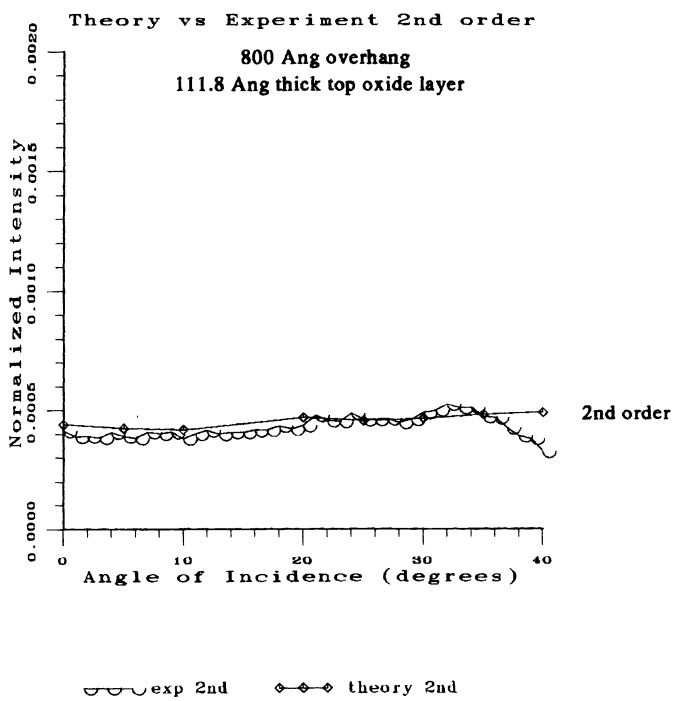


Figure 9. Experimental and theoretical data for 2nd order.

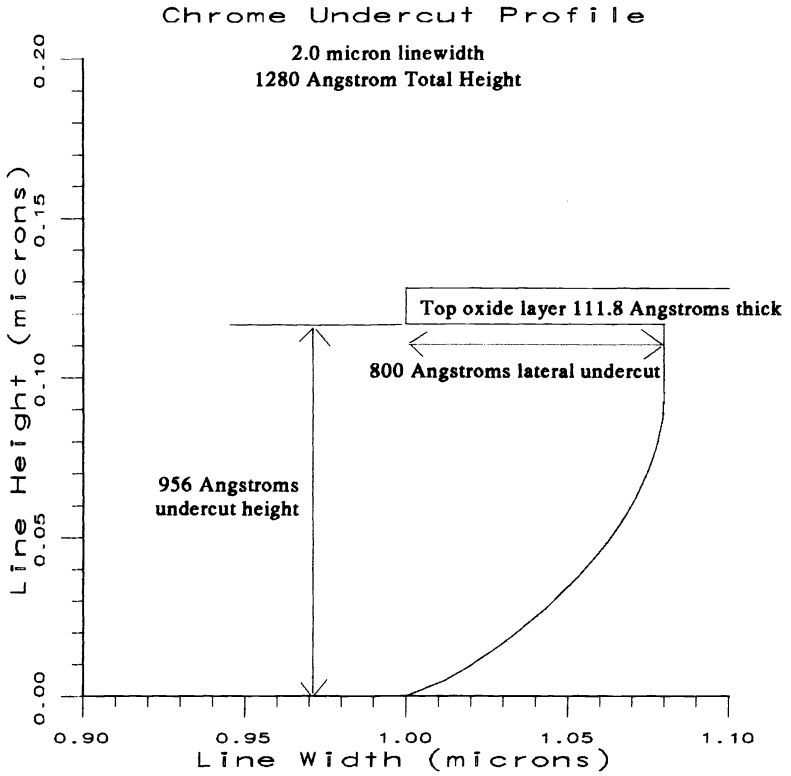


Figure 10. Best fit for the chrome line profile.

## 7.0 CONCLUSIONS AND FUTURE WORK

Scatterometry has been used to measure both the linewidth and the etch depth of phase shifted quartz gratings as well as the linewidth and line profile of attenuating chrome phase shift gratings. Comparison of the scatterometer and AFM measurements of the quartz gratings show that scatterometry results are within the measurement uncertainty of the AFM. Cross-sectional SEM photographs of the attenuating chrome grating would help to verify the line profile obtained through scatterometry. Unfortunately, that technique is destructive and would preclude further work on this photomask. Scatterometry offers a non-destructive way of determining undercut sidewall profiles. Commercially available AFMs are unable to probe this type of structure.

## 8.0 ACKNOWLEDGEMENTS

I would like to acknowledge Dr. Gregory Hughes of DuPont Photomasks, in Round Rock, Texas for supplying the attenuating chrome phase shift mask and supporting this work. I would also like to acknowledge the Intel Fellowship Foundation and the Intel Corporation for their support both financially and by providing me with a fast 486 PC. Additionally, I would like to thank Dr. Herschel Marchman of AT&T for supplying the original phase shift photomask and the attending AFM data.

## 9.0 REFERENCES

1. K.P. Bishop et al., "Grating line shape characterization using scatterometry," International Conference on the Application and Theory of Periodic Structures, Proc. SPIE vol. 1545 (1991).

2. S. M. Gaspar, "Characterization of photomask diffraction gratings using laser scatterometry," Masters Thesis, University of New Mexico, 1992.

3. R. Krukar, "A methodology for the use of diffracted scatter analysis to measure the critical dimension of periodic structures," Ph.D. Thesis, University of New Mexico, 1993.

4. S. H. Naqvi, et al., "Linewidth measurement of gratings on photomasks: a simple technique," Appl. Optics, April 1992.

5. J. M. Flaherty, "Inspection tools for every manufacturing phase", Test & Measurement World, p. 61, August 1993.

6. E. D. Palik, Handbook of Optical Constants of Solids, Academic Press Inc., San Diego, CA, 1985.

7. M. G. Moharram, T. K. Gaylord, "Three dimensional vector coupled wave analysis of planar grating diffraction," J. Optical Soc. of Am., Vol. 73 (9) Sep. 1983.

8. S. H. Naqvi, et al., "Scatterometry and the simulation of diffraction- based metrology", Microlithography World, pp. 5-12, July/Aug/Sep 1993.

9. B. Johs, et al., "Optical analysis of complex multilayer structures using multiple data types," presented at the International Conference on Thin Film Coatings, Grenoble, France, 6 June 1994.

10. F. D. Kalk, et al., "Attenuated phase-shifting photomasks fabricated from Cr-based embedded shifter blanks," presented at Photomask Japan 1994, Kanagawa Science Park, 22 April 1994.

11. GSolver Code, written and copyrighted by David Fluckinger.